Spatially Dependent Lattice Deformations for Dislocations at the Edges of Graphene

Chuncheng Gong,[†] Kuang He,[†] Alex W. Robertson,[†] Euijoon Yoon,[‡] Gun-Do Lee,[‡] and Jamie H. Warner*[,†]

[†]Department of Materials, University of Oxford, Parks Road, Oxford OX1 3PH, United Kingdom and [‡]Department of Materials Science and Engineering, Seoul National University, Seoul 151-742, Korea

ABSTRACT We show that dislocations located at the edge of graphene cause different lattice deformations to those located in the bulk lattice. When a dislocation is located near an edge, a decrease in the rippling and increase of the in-plane rotation occurs relative to the dislocations in the bulk. The increased in-plane rotation near the edge causes bond rotations at the edge of graphene to reduce the overall strain in the system. Dislocations were highly stable and remained fixed in their position even when located within a few lattice spacings from the edge of graphene. We study this behavior at the atomic level using aberration-corrected transmission electron microscopy. These results show detailed information about the behavior of dislocations in 2D materials and the strain properties that result.

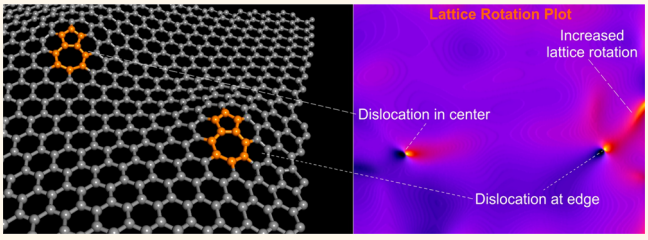

KEYWORDS: graphene · ripples · dislocations · defects · TEM

Dislocations play a key role in the plasticity of materials and their 3D deformations.[1−3] However, a century after it was first proposed, the real-time atomic-scale motion and annihilation of dislocations in 3D crystals is limited. Graphene is a one-atom-thick crystal with extraordinary electronic, magnetic and mechanical properties, which are easily affected by defects and dislocations.[4−10] The two-dimensional nature of graphene makes it a perfect candidate to study dislocations at the atomic level using transmission electron microscopy (TEM).[11−13]

High resolution TEM at an accelerating voltage of 80 kV drastically reduces knock-on damage to graphene and when chromatic aberration effects are reduced by monochromation of the electron source combined with aberration correction it is possible to obtain 80 pm spatial resolution.[14−17] Recent work showed that focusing an electron beam at 80 keV greatly increases the beam current density and it can controllably create defects in graphene including vacancies, dislocations and holes.[18] These defects are likely to be introduced by a complex chemical etching process, rather than direct knock-on sputtering. Recent work has studied the formation, migration and interaction between two dislocations at the atomic level using AC-TEM.[12,13]

Freely suspended graphene membranes can flex and buckle in *z*-direction.[19−21] Rippling is an out-of-plane distortion that is thought to help stabilize graphene.[22,23] It was theoretically predicted and later experimentally confirmed that dislocations lead to rippling in free-standing graphene sheets.[24−26] Dislocations can only be eliminated from the lattice of graphene by either annihilation from two opposite orientated dislocations or by migration to the edge of the lattice. The study of how dislocations behave close to the edge of graphene has not been experimentally examined and is the subject of this report. By using atomic resolution TEM we aim to understand the changes in the local strain properties around dislocations at the edge compared to those located in the bulk.

RESULTS AND DISCUSSIONS

Dislocations were created in graphene using a focused electron beam, as previously

* Address correspondence to Jamie.warner@materials.ox.ac.uk;.

Received for review October 21, 2014 and accepted December 8, 2014.

Published online December 15, 2014
10.1021/nn505996c

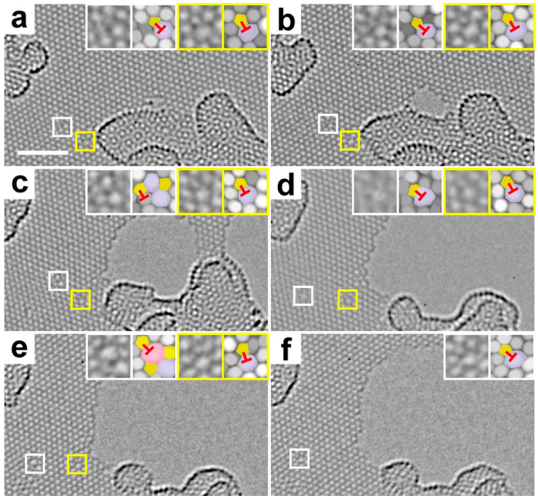

Figure 1. AC-TEM images showing the formation of dislocations near the edges of holes in graphene (magnified and maximum filtered views shown in the insets). Images were taken at times of (a) $t = 0$, (b) $t = 7$ min and 13 s, (c) $t = 12$ min and 41 s, (d) $t = 18$ min and 41 s, (e) $t = 25$ min and 24 s, (f) $t = 26$ min and 40 s. The scale bar in panels a is 2 nm. The color scheme in the maximum filtered images represents the number of carbon atoms in each ring, with 5 = yellow, 7 = blue, and 8 = pink.

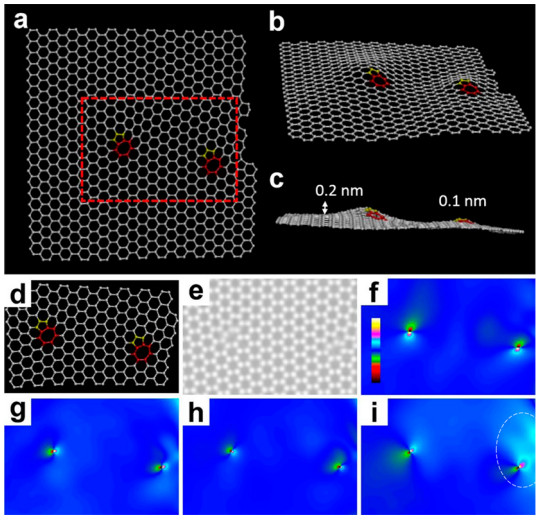

Figure 2. Density Functional Theory (DFT) simulations of ripples introduced by two dislocations located at different positions in graphene and their analysis. (a–c) DFT calculated atomic models of graphene with two dislocations (one in the center and one at the edge) (top, side and 3D views). Multislice images simulation (e) is applied to the atomic model of the red box in a (d). (f–i) Geometric phase analysis (GPA) strain plots (f) ε_{xx}, (g) ε_{xy}, (h) ε_{yy} and (i) rotation (radians) based on the image in e. Color scale bar used for GPA plots is in panel f (−1 to 1).

reported, and in some circumstances holes opened up next to the dislocations to provide an edge to interact with.[18] Figure 1a shows the formation of a hole and two pentagon-heptagon dislocation cores after the first exposure to the electron beam. Once the edge is created, the atoms on the edge are susceptible to sputtering by the 80 keV electrons. A second and third exposure to a focused electron beam for 60 s accelerated the sputtering of edge atoms after 10 and 15 min, before expanding the beam to image the area (Figure 1b–d). When the beam current density was reduced to $\sim 10^5$ e^1 nm^{-2} s^{-1} for imaging, the hole still kept on expanding, but at a very slow radial expansion rate of 1.4 pm s^{-1}. With the gradually sputtering of carbon atoms on the edge, the distance between the edge and the dislocations was reduced. The dislocation on the right side finally vanished 27 min after it was created (Figure 1e and f). The 55-77 and 555-7-8 defects on the left side, Figure 1c,e, are the reconstructed dislocation structure with a Stone–Wales rotation to the pentagon-heptagon structure.

The two dislocation cores highlighted in Figure 1 are not paired, *i.e.*, they do not have opposite direction, which means there must be at least two more dislocations within this local area. These two dislocations are highlighted because one is located near the edge, yellow box, and one is located further away from the edge, white box. This gives a good comparison between the behavior of a dislocation at the edge compared to the bulk. In order to understand what changes may result from a dislocation being located near the edge of graphene, we performed density functional theory (DFT) calculations of similar atomic structures.

Figure 2a–c shows the atomic model of two separated dislocations in graphene calculated by DFT. The simulation results indicate rippling is introduced by the two single dislocation cores. Furthermore, we notice that the size of the ripple introduced by the dislocation near the graphene edge is smaller than that introduced by the dislocation in the center of graphene. A rough value of the height of the two ripples is measured and shown in Figure 2c; the ripple introduced by the central dislocation is about twice (0.2 nm) that of the one located near the edge (0.1 nm). To further study the difference in lattice distortion introduced by two dislocations, we performed a multislice image simulation using the DFT atomic model (the red box region in Figure 2a), shown in Figure 2d, and then analyzed the image using geometric phase analysis (GPA). Applying GPA to HRTEM images is an effective way to identify and measure the out-of-plane distortion of graphene.[12,26–29] In our previous work, we demonstrated that the tilting of graphene lattice in *z*-direction is resolved as a noticeable decrease in lattice spacing in HRTEM images, which is the 2D projection of the 3D structure of graphene.[26] Theoretical simulations also indicated that C–C covalent bond lengths barely changed within the hexagonal rings. Thus, the "compression" in strain plots conducted by GPA can be interpreted as the lattice tilting of ripples, which is confirmed by the ε_{xx} strain plot in Figure 2f. The magnitude and location of the green region (corresponding to −0.2 in strain) in Figure 2f are in accordance with visual inspection of the atomic model in Figure 2c.

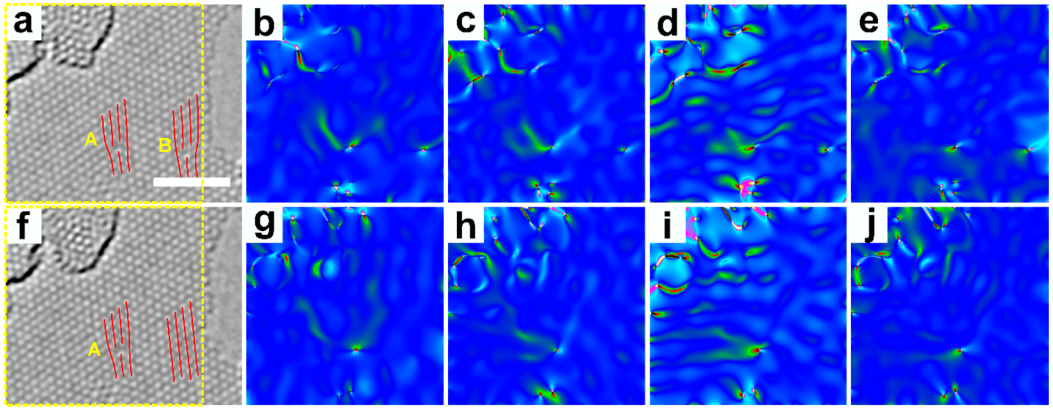

Figure 3. AC-TEM images of graphene with dislocations and their GPA plots. Smoothed AC-TEM images taken (a) before and (f) after Dislocation B disappeared. (b−e) GPA analysis based in panel a with (b) ε_{xx}, (c) ε_{xy}, (d) ε_{yy} and (e) rotation (radians). (g−j) GPA analysis based on panel f with (g) ε_{xx}, (h) ε_{xy}, (i) ε_{yy} and (j) rotation (radians). Time between panels a and f is 67 s. The scale bar in panel a is 2 nm.

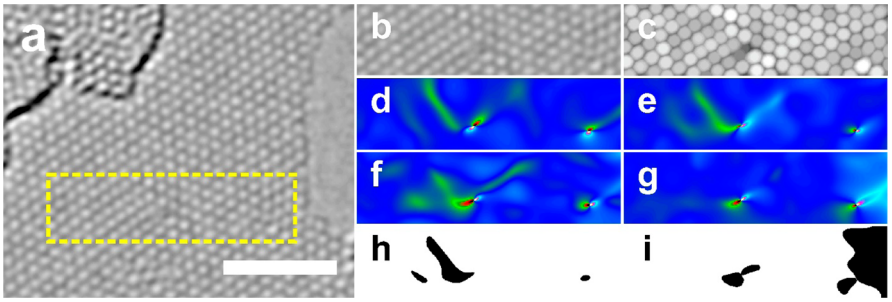

Figure 4. Smoothed and maximum filtered AC-TEM images and accompanying GPA plots of both dislocations cropped from Figure 3a. (a) Same TEM image as in Figure 3a with a dashed yellow rectangular box showing the cropped area presented in (b). (c) Maximum filtered image of panel b. (d−g) GPA plots of panel b, (d) ε_{xx}, (e) ε_{xy}, (f) ε_{yy} and (g) rotation (radians). (h) Binarized version of panel f, with the area where $\varepsilon_{yy} < -0.1$ being black, rest being white. (i) Binarized version of panel g, with the area where |rotation| >0.1 is black. The scale bar in panel a is 2 nm.

The rotation plot from GPA can also be used to measure the in-plane C−C bond rotation. The light blue region (corresponding to +0.2), indicated with a white dashed circle in Figure 2i, shows the area with significant bond rotation, which is mostly located between the right dislocation and the edge.

We now examine the experimental TEM images in Figure 3. Figure 3a shows both dislocations cause lattice distortion of the surrounding area (indicated with red lines). When the dislocation disappeared, the additional row of atoms and the lattice distortion were eliminated (Figure 3f). This result is further analyzed using GPA, as is shown in Figures 3b−e and 3g−j. The "compression" shown in GPA plots (ε_{xx}, ε_{xy} and ε_{yy}) in Figure 3 is due to the tilting of the graphene lattice from ripples. Figure 4 shows the GPA in higher magnification. The green region (corresponding to −0.2 in strain) in ε_{xx}, ε_{xy} and ε_{yy} strain plots represent the regions with significant change in lattice distance. In a similar way, the light blue and green colors in the rotation plots in Figure 3f,j and 4 indicate noticeable in-plane C−C bond rotation in these regions. We find the dislocation at the inner side of graphene (A) causes a much larger rippling of its surrounding area. The relative rippling area where $\varepsilon_{yy} < -0.1$ (black region in Figure 4h) introduced by Dislocation A (0.215 nm^2) is ~18 times that caused by Dislocation B (0.0120 nm^2). In the maximum filtered image (Figure 4c), the pentagon in Dislocation A and its neighboring hexagon are far less regular and less clearly resolved than those in Dislocation B, which also suggests Dislocation A causes a more severe out-of-plane distortion than B. On the contrary, the in-plane rotation (|rotation| > 0.1) caused by Dislocation A is only restricted in a small surrounding area, while that of dislocation B extends to a much larger area out to the edge. The strain introduced by the dislocation is accommodated differently if the dislocation is located near the edge of graphene. It gives rise to extensive in-plane rotation in the lattice between the dislocation and edge, rather than "hillocks" (large area of out-of-plane distortion) resulting from ripples.

Instead of a large area of C−C bond rotation, the lattice mismatch introduced by the dislocation can also be accommodated by defect structures at the edge. Bond rotation of edge atoms is the most frequently observed behavior, shown in Figure 5d and 6a. We analyzed two similar TEM images, one with Stone−Wales rotation on the edge (Figure 5d), the other without (Figure 5a). The rotated area (green and blue

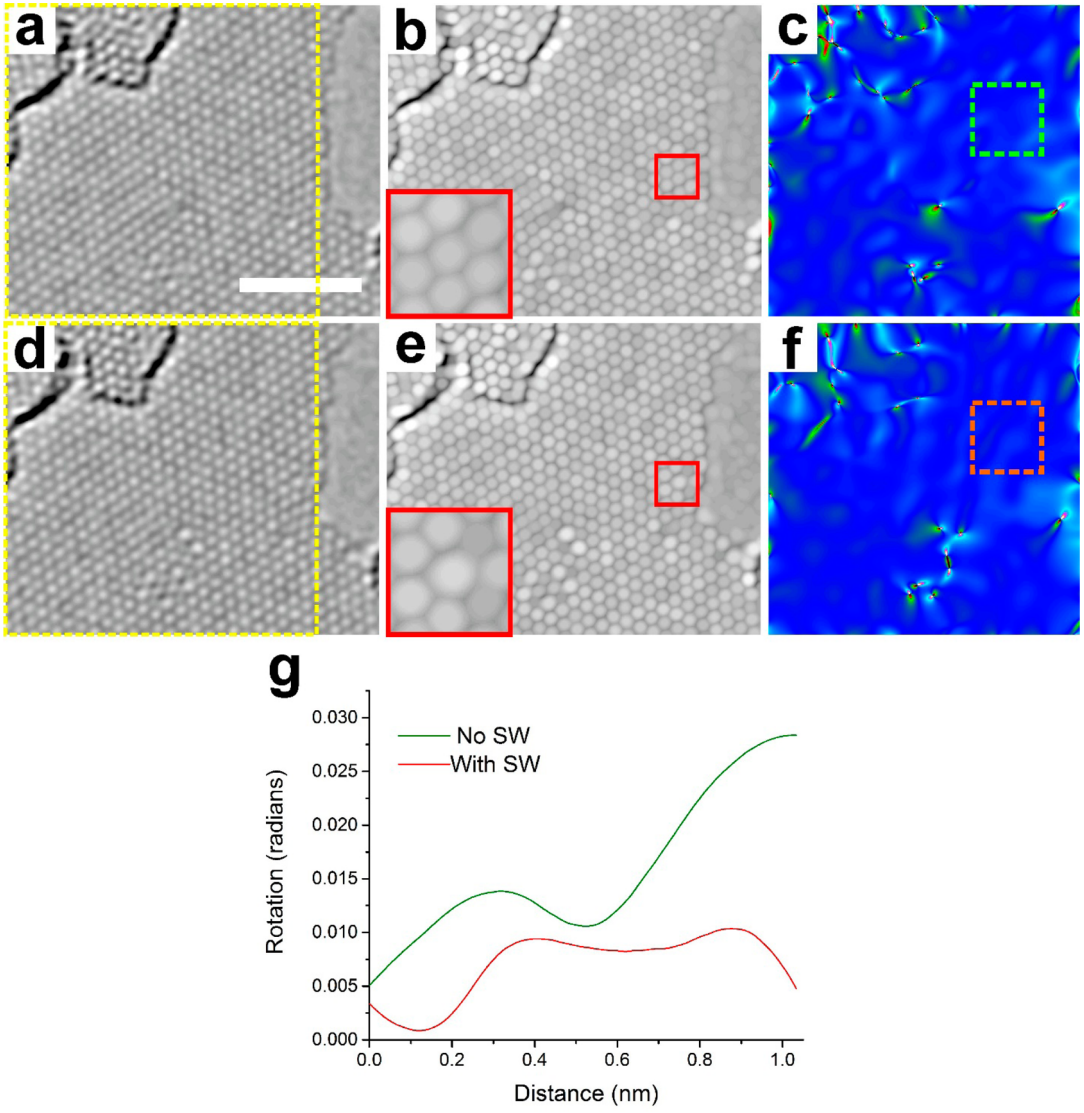

Figure 5. Bond rotations at the edge of graphene. AC-TEM images of the edge of graphene (a) before and (d) after a bond rotation at the edge. (b) Maximum filtered image of (a), with magnified view shown in the inset. (c) Rotation plot from GPA of the cropped area in panel a. (e) Maximum filtered image of (d), with magnified view shown in the inset. (f) Rotation plot from GPA of the cropped area in panel d. (g) Boxed line profile from the dashed square in panel sc and f showing the average rotation over vertical 158 pixels corresponding to a distance of 0.65 nm. The scale bar in panel a is 2 nm.

area in rotation plots) around the dislocation core reduced significantly with the Stone–Wales rotation on the edge (Figure 5c,f). We also measured the mean value of rotation in the vertical direction of the same region away from the dislocation in both images. The result shown in Figure 5g reveals that the existence of Stone Wales rotation on the graphene edge can lead to the decrease of rotation in the area far from the dislocation core.

To study the time-dependent edge structure with the dislocation nearby, we took in total 54 TEM images over 608 s, with 11 s per image on average. About 40 images were taken when the dislocation was near the edge and the remaining 14 were taken after the dislocation disappeared by migrating to the edge. Along with the bond rotations, various other types of defects were also found on the edge, which are listed by the frequency-of-occurrence in the 40 images in descending order. The bond rotation was present in 31 out of 40 images (Figure 6a) in the exact same position. The individual pentagon was the second most frequently occurring structure (18 times), shown in Figure 6b. The 5-7-5 reconstructed edge (Figure 6c) and the double bond rotated structure (Figure 6d) both occurred 6 times. And the 555–8 structure (Figure 6e) which might go through several rotations and edge reconstructions, showed up 5 times. After the dislocation disappeared, none of these structures appeared in the remaining 14 images for 2 min 9 s as is shown in Figure 3f, indicating they are primarily caused by the dislocation. It is worth noting that bond rotations and defects can still occur at the edge of holes, without

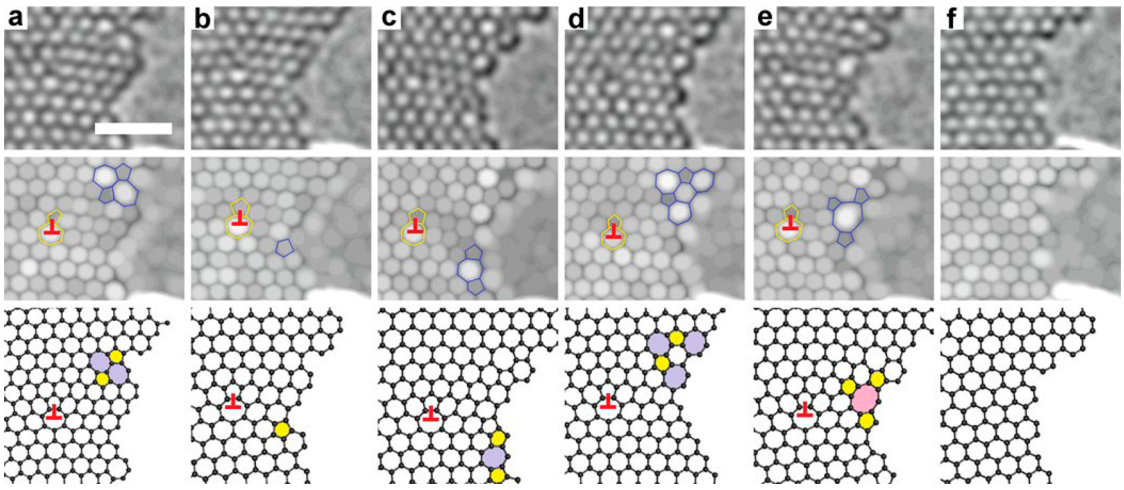

Figure 6. Different kinds of defects found at the edge of graphene when a dislocation is nearby. AC-TEM images (with corresponding maximum filtered images below) showing (a) Bond rotation, (b) an isolated pentagon, (c) a 5−7−5 structure, (d) double bond rotation structure, (e) a 555−8 structure. The scale bar in panel a is 1 nm. The color scheme in the atomic models represents the number of carbon atoms in each ring, with 5 = yellow, 7 = blue and 8 = pink.

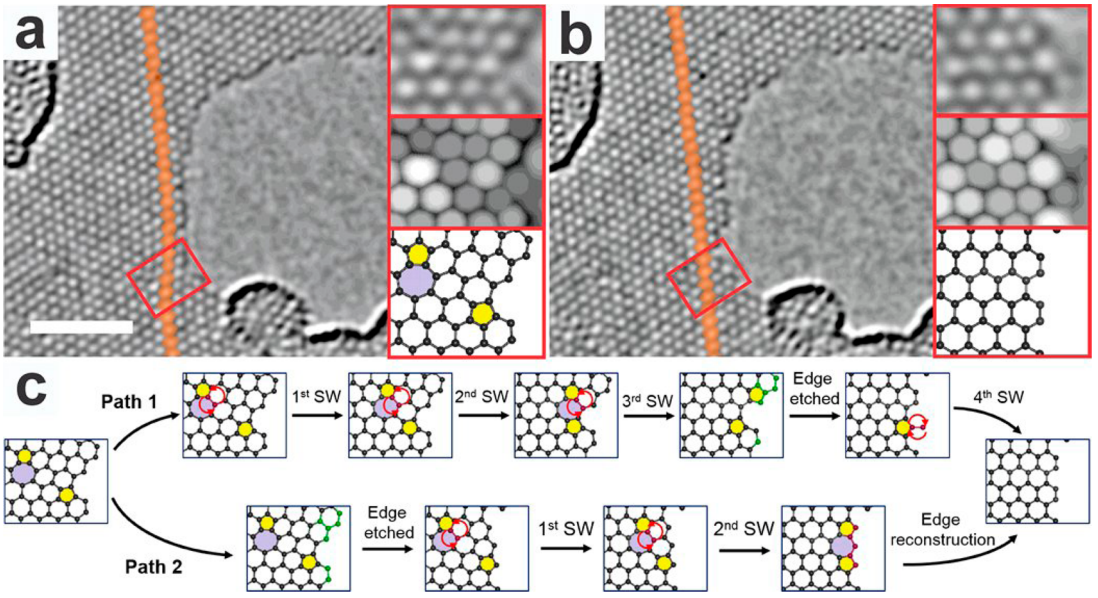

Figure 7. AC-TEM images taken (a) before and (b) after a dislocation disappeared, with magnified, maximum filtered views and atomic models presented in the insets. The time between two images is 67 s. The scale bar in panel a is 2 nm. (c) Atomic models showing two possible paths of how the dislocation glides to the edge. The color scheme in atomic models represent the number of carbon atoms in each ring, with 5 = yellow, 7 = blue. Orange lines indicate the distortion of the graphene lattice line is released when the dislocation is gone.

nearby dislocations, it is just that the frequency of occurrence drops dramatically. However, small holes have curvature effects, which are absent from large holes, and this can also increase the occurrence of bond rotations at the edge. The hole we examined in Figure 6 was large enough that curvature did not play a major role.

In Figure 7 we discuss some of the final structural pathways that could lead to the dislocation migrating to the edge. There are numerous ways in which the dislocation can make this journey, and we can therefore only limit our discussion to the two simplest pathways. Figure 7a shows the dislocation close to the edge, with the orange line indicting the curvature of the lattice, and in Figure 7b, the dislocation is gone and so too has the curvature. The disappearance of the dislocation between Figure 7a.b can be explained by several glides *via* bond rotation. Figure 7c gives two possible explanations. In path 1, three bond rotations occur first. As a result, the heptagon in the dislocation core disappears to the edge and the lattice distortion is released. After the sputtering of the green atoms by the electron beam, the atoms highlighted in red are rotated to form a 6 member ring. Figure 7c also shows a second path in which green atoms are etched first, followed by two bond rotations. Consequently, the

lattice distortion is released and a 5-7-5 edge structure is formed. 5-7-5 then reconstructs into three hexagons with an additional carbon atom. Both pathways presented in Figure 7 require the dislocation to move along its glide plane through at least two bond rotations to reach the edge. Prior to this the dislocation remained fixed in its position. Density Functional Theory (DFT) calculations, (see Supporting Information Figure S4), indicate that it is energetically favorable for the dislocation to glide toward the edge of graphene once it is close enough.

CONCLUSIONS

The ability to track in real time two dislocations in graphene, one near a hole and another within the bulk, has allowed us to understand the local strain properties and how the dislocation affects the edge of graphene. The dislocation near the edge causes larger in-plane C−C bond rotations at the expense of reduced "hillocks" caused by out-of-plane distortions. Bond rotations at the graphene edge help alleviate the strain from the in-plane lattice rotations caused by nearby dislocations. Dislocations remained localized in their positions even to within a few lattice spacings of the edge, before it either glides toward the edge or the edge is sputtered all the way to the dislocation and it then disappears. These results provide important fundamental insights into the behavior of edge dislocations in graphene in the bulk and near the edge. The strain properties induced by the dislocation are substantially different when near the edge and highlight the sensitivity to the local structural environment.

METHODS

Synthesis of Graphene. Monolayer graphene was synthesized by atmospheric pressure chemical vapor deposition (CVD) method using a melted copper sheet as the catalytic as previously reported.[30] The high purity copper foil (Alfa Aesar, Puratonic 99.999% pure, 0.1 mm thick) of ~1 cm^2 was placed on the molybdenum piece of same size (Alfa Aesar, 99.95% pure, 0.1 mm thick), which were both loaded into a 1 in. quartz tube in the CVD system. Molybdenum act as a stable wetting layer to prevent liquid copper from balling. A total of 100 sccm H_2/Ar (20% H_2 in Ar), 100 sccm CH_4 (1% CH_4 in Ar) and 200 sccm 100% Ar were flowed for 30 min. CH_4 flow was switched off before increasing hot−zone temperature to 1090 °C. Once the temperature reached 1090 °C, the quartz tube was moved from the room temperature zone to the center of heating zone and annealed for 30 min. The flow of H_2/Ar was then reduced to 80 sccm, and 10 sccm of 1% CH_4 in Ar was added for 90 min for graphene growth. After growth, the quartz was removed from the heating zone for rapid cooling in the air with CH_4 off.

Transfer. A PMMA scaffold (8 wt % in anisole, 495k molecular weight) was spin−coated onto the graphene sheet at 4700 rpm for 60 s and then baked at 180 °C for 90 s to solidify. Afterward the sample was made up of a molybdenum/copper/graphene/PMMA stack. The copper layer were etched by floating the sample on the mixed solution of iron(III) chloride and hydrochloride, leaving a floating graphene−PMMA film on the top after 48 h. The film was collected using a clean glass slide and transferred onto the surface of the DI water for 30 min wash away remaining iron(III) chloride. To further dissolve excess iron chloride, the sample was transferred onto a 10% hydrogen chloride solution for 5 min, before rinsed again in the DI water for 30 min. A holey Si_3N_4 TEM grid (Agar Scientific Y5358) was mounted onto an adhesive silicon chip and was used to scoop up the floating graphene/PMMA film. Afterward, the grid on the silicon chip was moved onto a glass slide and dried in the air for 24 h and subsequently baked at 150 °C to relax for 15 min. The grid on the silicon chip was then cured at 350 °C for 12 h to burn out PMMA, leaving only graphene on the holey Si_3N_4 grid.

Electron Microscopy. HRTEM images were taken at an accelerating voltage of 80 kV, using Oxford's JEOL JEM-2200MCO field emission transmission electron microscope with a CEOS image corrector.[12] Defects were introduced using a focused electron beam according to our previously reported procedure.[18] TEM images were processed using ImageJ. Smoothing of images was achieved by using a Gaussian blur filter in ImageJ. The ImageJ maximum filter was also used in some instances. Geometric Phase Analysis was performed using the FRWRTools plugin for Digital Micrograph written by C. Koch.

Density Functional Theory (DFT) Calculations. We perform DFT total energy calculations to obtain the optimized structures of edges and dislocation-introduced ripples in graphene. The DFT calculations are performed within the generalized gradient approximation of Perdew−Burke−Ernzerhof (PBE) functional using Vienna ab initio simulation package (VASP) code.[31,32] The basis set contains plane waves up to an energy cutoff of 400 eV. We perform the simulations with a graphene patch containing 706 carbon atoms for all energy and structure study. The unit cell is constructed by removing 46 carbon atoms from pristine graphene of 752 carbon atoms to create the hole and edges. The unit cell is periodically repeated in the lateral direction and contains the vacuum region of 30 Å. We choose only one k point, the Γ point because the unit cell is enough large. When structural relaxations are performed, the structure is fully relaxed until the force on each atom is smaller than 0.02 eV/Å.

Conflict of Interest: The authors declare no competing financial interest.

Acknowledgment. J.H.W. thanks the support from the Royal Society. C.G. thanks the support form Clarendon Fund Scholarship. G.-D.L. and E.Y. acknowledge support from the Supercomputing Center/Korea Institute of Sceince and Technology Information with supercomputing resources (KSC-2014-C3-009), from BK21 plus program, and from the National Research Foundation of Korea (NRF) grant funded by the Korea Government (RIAM No. 2010-0012670, MSIP No. 20080061900).

Supporting Information Available: Extra TEM image and analysis of a dislocation near the edge of graphene, Density Functional Theory (DFT) calculations of the dislocation glide near the edge. This material is available free of charge *via* the Internet at http://pubs.acs.org.

REFERENCES AND NOTES

1. Volterra, V. Sull' Equilibrio Dei Corpi Elastici Più Volte Connessi. *Nuovo Cim. Ser. 5* **1905**, *10*, 361–385.
2. Read, W. T.; Shockley, W. Dislocation Models of Crystal Grain Boundaries. *Phys. Rev.* **1950**, *78*, 275–289.
3. Hull, D. Introduction to Dislocations. *Am. J. Phys.* **1968**, *36*, 174.
4. Novoselov, K. S.; Geim, A. K.; Morozov, S. V.; Jiang, D.; Zhang, Y.; Dubonos, S. V.; Grigorieva, I. V.; Firsov, A. A. Electric Field Effect in Atomically Thin Carbon Films. *Science* **2004**, *306*, 666–669.
5. Lee, C.; Wei, X.; Kysar, J. W.; Hone, J. Measurement of the Elastic Properties and Intrinsic Strength of Monolayer Graphene. *Science* **2008**, *321*, 385–388.
6. Yazyev, O. Magnetism in Disordered Graphene and Irradiated Graphite. *Phys. Rev. Lett.* **2008**, *101*, 037203.

7. Ishigami, M.; Chen, J. H.; Cullen, W. G.; Fuhrer, M. S.; Williams, E. D. Atomic Structure of Graphene on SiO_2. *Nano Lett.* **2007**, *7*, 1643–1648.
8. Castro Neto, a. H.; Peres, N. M. R.; Novoselov, K. S.; Geim, a. K. The Electronic Properties of Graphene. *Rev. Mod. Phys.* **2009**, *81*, 109–162.
9. Bae, S.; Kim, H.; Lee, Y.; Xu, X.; Park, J.-S.; Zheng, Y.; Balakrishnan, J.; Lei, T.; Kim, H. R.; Song, Y. I.; *et al.* Roll-to-Roll Production of 30-Inch Graphene Films for Transparent Electrodes. *Nat. Nanotechnol.* **2010**, *5*, 574–578.
10. Krasheninnikov, A. V.; Lehtinen, P. O.; Foster, A. S.; Pyykkö, P.; Nieminen, R. M. Embedding Transition-Metal Atoms in Graphene: Structure, Bonding, and Magnetism. *Phys. Rev. Lett.* **2009**, *102*, 126807.
11. Hashimoto, A.; Suenaga, K.; Gloter, A.; Urita, K.; Iijima, S. Direct Evidence for Atomic Defects in Graphene Layers. *Nature* **2004**, *430*, 17–20.
12. Warner, J. H.; Margine, E. R.; Mukai, M.; Robertson, A. W.; Giustino, F.; Kirkland, A. I. Dislocation-Driven Deformations in Graphene. *Science* **2012**, *337*, 209–212.
13. Lehtinen, O.; Kurasch, S.; Krasheninnikov, a V; Kaiser, U. Atomic Scale Study of the Life Cycle of a Dislocation in Graphene from Birth to Annihilation. *Nat. Commun.* **2013**, *4*, 2098.
14. Hawkes, P. W. Aberration Correction Past and Present. *Philos. Trans. R. Soc,. A* **2009**, *367*, 3637–3664.
15. Meyer, J. C.; Kisielowski, C.; Erni, R.; Rossell, M. D.; Crommie, M. F.; Zettl, a. Direct Imaging of Lattice Atoms and Topological Defects in Graphene Membranes. *Nano Lett.* **2008**, *8*, 3582–3586.
16. Ramasse, Q. M.; Zan, R.; Bangert, U.; Boukhvalov, D. W.; Son, Y. W.; Novoselov, K. S. Direct Experimental Evidence of Metal-Mediated Etching of Suspended Graphene. *ACS Nano* **2012**, *6*, 4063–4071.
17. Robertson, A. W.; Warner, J. H. Atomic Resolution Imaging of Graphene by Transmission Electron Microscopy. *Nanoscale* **2013**, *5*, 4079–4093.
18. Robertson, A. W.; Allen, C. S.; Wu, Y. a; He, K.; Olivier, J.; Neethling, J.; Kirkland, A. I.; Warner, J. H. Spatial Control of Defect Creation in Graphene at the Nanoscale. *Nat. Commun.* **2012**, *3*, 1144.
19. Meyer, J. C.; Geim, A. K.; Katsnelson, M. I.; Novoselov, K. S.; Booth, T. J.; Roth, S. The Structure of Suspended Graphene Sheets. *Nature* **2007**, *446*, 60–63.
20. Fasolino, A.; Los, J. H.; Katsnelson, M. I. Intrinsic Ripples in Graphene. *Nat. Mater.* **2007**, *6*, 858–861.
21. Kirilenko, D. A.; Dideykin, A. T.; Van Tendeloo, G. Measuring the Corrugation Amplitude of Suspended and Supported Graphene. *Phys. Rev. B - Condens. Matter Mater. Phys.* **2011**, *84*, 235417.
22. Lui, C. H.; Liu, L.; Mak, K. F.; Flynn, G. W.; Heinz, T. F. Ultraflat Graphene. *Nature* **2009**, *462*, 339–341.
23. Bonilla, L. L.; Carpio, A. Model of Ripples in Graphene. *hys. Rev. B: Condens. Matter Mater. Phys.* **2012**, *86*, 195402.
24. Liu, Y.; Yakobson, B. I. Cones, Pringles, and Grain Boundary Landscapes in Graphene Topology. *Nano Lett.* **2010**, *10*, 2178–2183.
25. Yakobson, B. I.; Ding, F. Observational Geology of Graphene, at the Nanoscale. *ACS Nano* **2011**, *5*, 1569–1574.
26. Warner, J. H.; Fan, Y.; Robertson, A. W.; He, K.; Yoon, E.; Lee, G. Do. Rippling Graphene at the Nanoscale through Dislocation Addition. *Nano Lett.* **2013**, *13*, 4937–4944.
27. Hytch, M. J.; Snoeck, E.; Kilaas, R. Quantitative Measurement of Displacement and Strain Fields from HREM Micrographs. *Ultramicroscopy* **1998**, *74*, 131–146.
28. Moodie, A. F. Numerical Evaluation of N-Beam Wave Functions in Electron Scattering by the Multi-Slice Method. *Acta Crystallogr., Sect. A* **1970**, *30*, 280–290.
29. Cowley, J. M.; Moodie, A. F. The Scattering of Electrons by Atoms and Crystals. I. A New Theoretical Approach. *Acta Crystallogr.* **1957**, *10*, 609–619.
30. Wu, Y. a; Fan, Y.; Speller, S.; Creeth, G. L.; Sadowski, J. T.; He, K.; Robertson, A. W.; Allen, C. S.; Warner, J. H. Large Single Crystals of Graphene on Melted Copper Using Chemical Vapor Deposition. *ACS Nano* **2012**, *6*, 5010–5017.
31. Perdew, J.; Burke, K.; Ernzerhof, M. Generalized Gradient Approximation Made Simple. *Phys. Rev. Lett.* **1996**, *77*, 3865–3868.
32. Kresse, G. Efficient Iterative Schemes for Ab Initio Total-Energy Calculations Using a Plane-Wave Basis Set. *Phys. Rev. B* **1996**, *54*, 11169–11186.
33. Lee, G. Do; Wang, C. Z.; Yoon, E.; Hwang, N. M.; Ho, K. M. Vacancy Defects and the Formation of Local Haeckelite Structures in Graphene from Tight-Binding Molecular Dynamics. *hys. Rev. B: Condens. Matter Mater. Phys.* **2006**, *74*, 245411.